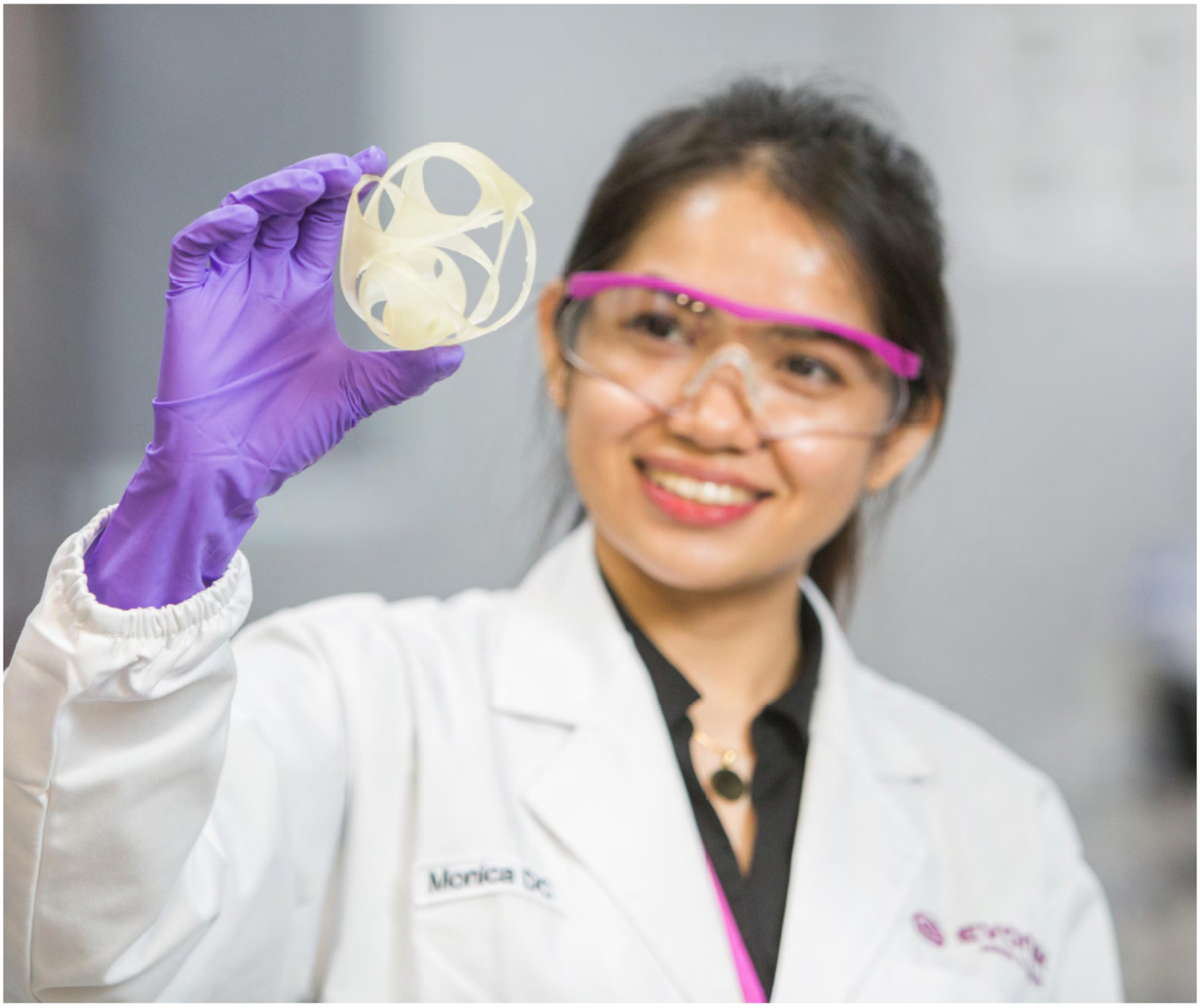

Pushing the boundaries of chemistry? It takes #HumanChemistry

Make your curiosity and talent as a chemist matter to the world with a specialty chemicals leader. Together, we combine cutting-edge science with engineering expertise to create solutions that answer real-world problems. Find out how our approach to technology creates more opportunities for growth, and see what chemistry can do for you at:

evonik.com/career

EVONIK
Leading Beyond Chemistry

ADVANCED MATERIALS
www.advmat.de

A Bioresorbable Dynamic Pressure Sensor for Cardiovascular Postoperative Care

Han Ouyang, Zhe Li, Min Gu, Yiran Hu, Lingling Xu, Dongjie Jiang, Sijing Cheng, Yang Zou, Yu Deng, Bojing Shi, Wei Hua, Yubo Fan,* Zhou Li,* and Zhonglin Wang*

Bioresorbable electronics that can be absorbed and become part of the organism after their service life are a new trend to avoid secondary invasive surgery. However, the material limitation is a significant challenge. There are fewer biodegradable materials with pressure-sensitive properties. Here, a pressure sensor based on the triboelectric effect between bioabsorbable materials is reported. This effect is available in almost all materials. The bioresorbable triboelectric sensor (BTS) can directly convert ambient pressure changes into electrical signals. This device successfully identifies abnormal vascular occlusion events in large animals (dogs). The service life of the BTS reaches 5 days with a high service efficiency (5.95%). The BTS offers excellent sensitivity (11 mV mmHg^{-1}), linearity ($R^2 = 0.993$), and good durability (450 000 cycles). The antibacterial bioresorbable materials (poly(lactic acid)–(chitosan 4%)) for the BTS can achieve 99% sterilization. Triboelectric devices are expected to be applied in postoperative care as bioresorbable electronics.

1. Introduction

Implantable biosensors improve patient care and disease management due their ability to continue monitoring vital physiological signals in situ.[1–3] However, most existing implantable sensors must be removed or replaced via an invasive, complex surgery at the end of the service life.[4] Implantable biodegradable electronic devices that can be absorbed or degraded in vivo are a new trend to avoid secondary invasive surgery.[2,5] A series of breakthroughs have been achieved for biodegradable devices in wireless intracranial pressure monitoring,[3] abdominal cavity detection,[6] and tissue strain sensing.[7] These works suggest the promising future of biodegradable sensors in vital physiological signal monitoring, postoperative care, rehabilitation, and regenerative medicine.

An implantable biodegradable sensor is often required to be implanted in vivo and to be directly conformable with soft tissues and organs.[8] Thus, favorable mechanical properties, flexibility, and biocompatibility are essential for these sensors.[6,9] Fortunately, many degradable polymers,[10] metals and oxides with good electrical performance have been explored for bioelectronics.[11] Some critical parameters for biodegradable implantable devices have been optimized in parallel with the development of materials, electronics, and advanced manufacturing technologies.[12]

Dr. H. Ouyang, Prof. B. Shi, Prof. Y. Fan
Key Laboratory for Biomechanics and Mechanobiology
of Chinese Education Ministry
Beijing Advanced Innovation Centre for Biomedical Engineering
School of Biological Science and Medical Engineering
Beihang University
Beijing 100083, China
E-mail: yubofan@buaa.edu.cn

Dr. H. Ouyang, Dr. Z. Li, Dr. L. Xu, D. Jiang, Dr. Y. Zou, Prof. Z. Li, Prof. Z. L. Wang
CAS Center for Excellence in Nanoscience
Beijing Key Laboratory of Micro-Nano Energy and Sensor
Beijing Institute of Nanoenergy and Nanosystems
Chinese Academy of Sciences
Beijing 100083, China
E-mail: zli@binn.cas.cn

Dr. Z. Li
Beijing Institute of Technology
Institute of Engineering Medicine
School of Life Science
Beijing 100081, P. R. China

Prof. M. Gu, Dr. Y. Hu, S. Cheng, Y. Deng, Prof. W. Hua
The Cardiac Arrhythmia Center
State Key Laboratory of Cardiovascular Disease
National Clinical Research Center of Cardiovascular Diseases
Fuwai Hospital
National Center for Cardiovascular Diseases
Chinese Academy of Medical Sciences and Peking Union
Medical College
Beijing 100037, China
E-mail: drhuaweifw@sina.com

Dr. L. Xu, D. Jiang, Dr. Y. Zou, Prof. Z. Li, Prof. Z. L. Wang
School of Nanoscience and Technology
University of Chinese Academy of Sciences
Beijing 100049, China

Prof. Z. Li, Prof. Z. L. Wang
Center on Nanoenergy Research School of Physical
Science and Technology
Guangxi University
Nanning 530004, P. R. China

The ORCID identification number(s) for the author(s) of this article can be found under https://doi.org/10.1002/adma.202102302.

DOI: 10.1002/adma.202102302

Currently, some barriers still have to be overcome for postoperative care applications. 1) The service life of most implanted biodegradable sensors cannot meet the postoperative care cycle, which is often 4–10 days.[13] Commonly used biodegradable packaging materials have a short degradation time,[4,14] such as poly(vinyl alcohol), silk fibroin, and poly(lactic-*co*-glycolic acid). Long-term biodegradable encapsulating material design is a critical issue. 2) The surface antibacterial strategies used in implants are not suitable for degradable devices. Substances inside the devices will be exposed in vivo during the degradation process. 3) Ultralow power consumption is a necessity due to the limited energy supply matching biodegradable devices.[15]

Recently, self-powered sensors based on triboelectric and piezoelectric nanogenerators[16] for wearable/implantable applications[17] have been rapidly developed due to their wide range of material choices, simple production processes, and high output voltages.[18] The triboelectric effect of biodegradable materials has been proven,[19] and the maximum output voltage can reach several volts or even hundreds of volts when driven by external forces. Thus, biodegradable triboelectric devices are expected to be made into biodegradable sensors for disease diagnosis in vivo after overcoming key challenges such as sensitivity, linearity and stability. In addition, the triboelectric effect breaks through the limitation of the pressure-sensitive principle for materials and expands the usable material library.[20]

Here, we propose an implantable bioresorbable self-powered sensor based on the triboelectric effect (BTS). The BTS directly converts biomechanical movement into electrical signals and successfully identify vascular occlusion events in large animals (dogs). In addition, the BTS is endowed with good antibacterial properties. We designed antibacterial bioresorbable materials for the BTS, poly(lactic acid)–(chitosan 4%) (PLA/C), which can achieve 99% sterilization. As a mechanical sensor, the BTS has a sensitivity of up to 11 mV $mmHg^{-1}$. The good linearity (R^2 = 99.3%) due to the air spacer structure causes the mechanical properties of the BTS to comply with the ideal gas law. The BTS can be absorbed and become part of the organism after the service life. Its service life has reached 5 days. This self-powered sensor is the first to achieve full bioresorbability in vivo and show the ability to identify abnormal disease events. These findings show that triboelectric pressure sensing is a new technology able to compete with piezoelectricity, etc., in bioresorbable applications.

2. Results and Discussion

2.1. Overview of the BTS

The core component of the BTS is two triboelectric layers that convert mechanical motion signals into electrical signals (**Figure 1**a,b). An external encapsulation layer prevents internal components of the sensor from being invaded by the liquid environment. One PLA/C film with a nanostructured surface is used as a triboelectric layer. A magnesium (Mg) layer deposited on the backside serves as an electrode. In addition, Mg has been deposited on the other PLA/C film to obtain a nanostructured metal layer for use as an electrode and a triboelectric layer simultaneously. The entire device is packaged in PLA/C. Elastic poly(1,8-octane diol-*co*-citric acid) (POC) is used as the adhesive layer (Figure S1 and Table S1, Supporting Information).

The two triboelectric layers are in contact under an external force, and the electrons on the Mg surface are transferred to the PLA/C surface due to contact electrification. The distance between the triboelectric layers changes due to variations in external forces, at which point the sensor outputs an electrical signal associated with the mechanical motion[21] (Figure 1c; and Note S1, Supporting Information). The surface nanostructure can increase the actual contact area when the friction layer works, leading to a larger electrical signal to improve the sensitivity of the sensor (Figure S2, Supporting Information).

Here, we have designed an air spacer structure. The separation of the triboelectric layers depends on the air in the middle. This kind of air spacer structure causes the mechanical properties of the BTS to comply with the ideal gas law. Therefore, the pressure change detected by the device and the open-circuit voltage output have good linearity (Note S2, Supporting Information)

$$\Delta P = \frac{\mathrm{n}RT\varepsilon_0}{x_0\sigma}U_{\mathrm{oc}} \tag{1}$$

Here, ΔP is pressure change. n is the number of moles. R is universal gas constant. T is the temperature. ε_0 is the permittivity of the vacuum. x_0 is initial displacement. σ is surface charge density. The U_{oc} is open-circuit voltage.

2.2. In Vitro Characterization of the BTS

To demonstrate the excellent mechanical sensing performance, the BTS was attached to the throat to monitor vocal cord vibration. A voltage signal of 4–9 mV was obtained when the volunteer pronounced "B" "T" and "S" (**Figure 2**a). After short-time Fourier transform analysis of the signal, the changes in the pronunciation of different letters can be clearly identified. Similar results from the two trials with accents also confirmed the device's good reliability. The BTS can detect 1 kHz vibration signals from a small loudspeaker and convert them to electrical signals in real time. The response time is as fast as 0.5 ms (Figure S3a–f, Supporting Information).

Stable operation in the body is essential for the BTS as an implantable sensor. We measured the output stability in non-liquid environments. The maximum output of the BTS can reach 4.2 V when driven by a linear motor (20 N). The output remains stable under the stimulation of a 1–5 Hz mechanical force (Figure 2b). In addition, the output also remains stable under 450 000 saturated mechanical stimuli (Figure 2c). Here, ≈4 cycles can be observed in the cycle window of 3 s. A linear motor was employed as a source of mechanical stimuli (20 N, 1.35 Hz) for a long-term stability test. The output voltage of the BTS was measured at intervals of 18.5 h which is approximately every 9×10^4 cycles.

The BTS output performance is the most important indicator. A pressure testing system was built to calibrate the sensitivity of the BTS (Figure 2d). The BTS output increases with increasing driving pressure (0–170 mmHg) and finally reaches

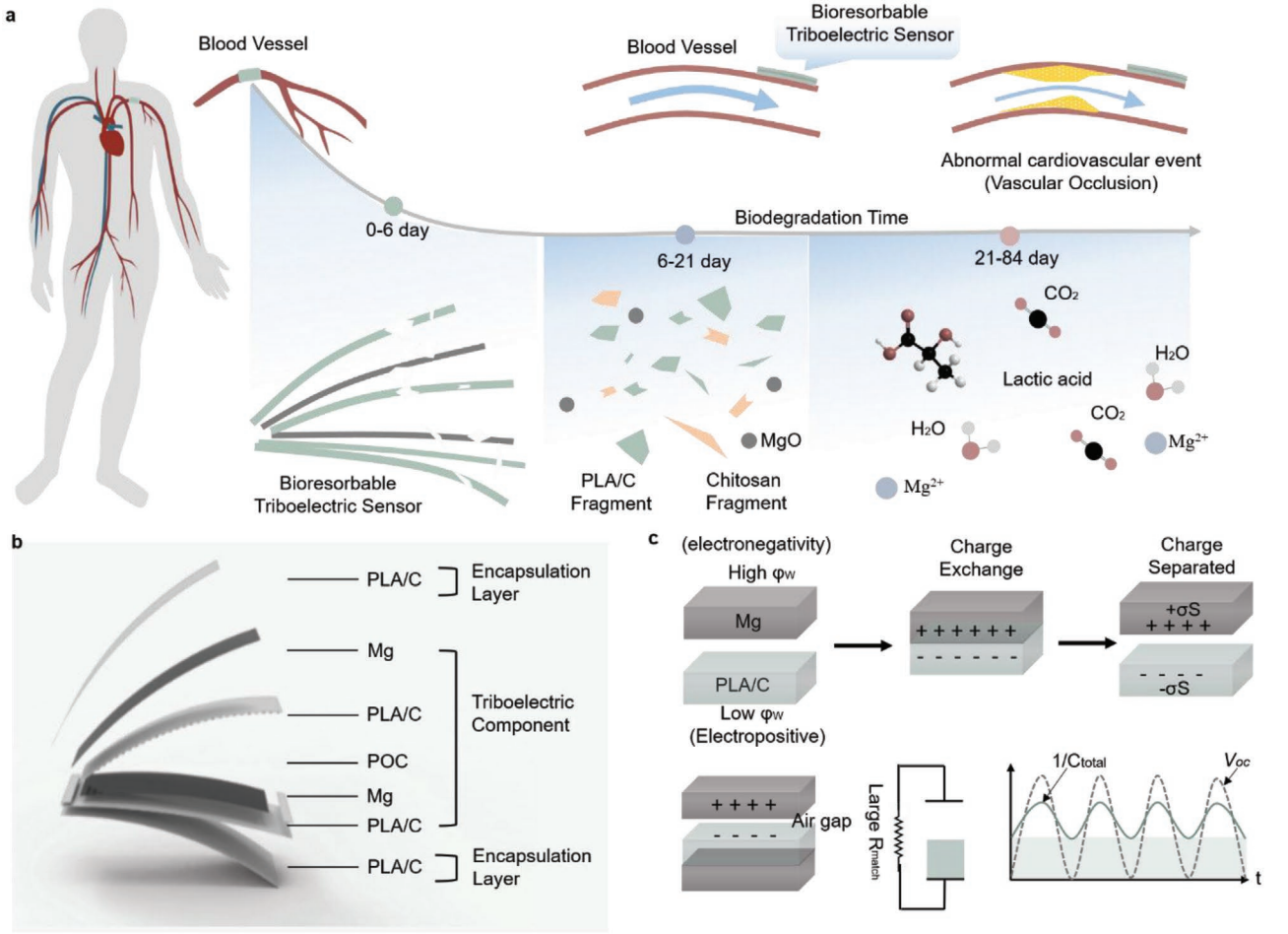

Figure 1. Overview and principle of the BTS. a) Illustration of the BTS. b) Structure of the BTS. c) Principle of the BTS based on contact electrification and electrostatic induction.

the full level of 2 V. This pressure range covers almost all pressures in vivo. The BTS sensitivity reaches 11 mV $mmHg^{-1}$, and the linearity is close to $R^2 = 99.3\%$ (Figure 2e,f).

2.3. Degradation Performance of the BTS

To measure the BTS mass decreases with time, the BTS was placed in a constant temperature phosphate buffer saline (37 °C, 1 × PBS). The chain splitting reaction preferentially occurs in the amorphous region during the hydrolysis and degradation of PLA/C. PLA/C break into polymer fragments of PLA and polymer fragments of chitosan after swelling after the chain breaks. These fragments degrade into H_2O, CO_2, lactic acid, etc., which are eventually absorbed in vivo (**Figure 3**a; and Note S3, Supporting Information). The mass of the BTS was 98.9 ± 0.42% compared to the original mass after 3 days. The Mg metal layers inside the device were degraded on the 8th day, and the mass of the BTS was reduced to 96.3 ± 0.78%. The BTS was completely degraded after 63–84 days in vitro (Figure 3b; and Figure S4a,b, Supporting Information).

After ≈4–8 days, the device output suddenly dropped to ≈1 V in nonliquid environment (Figure 3c). At ≈4–8 days, damage to the device encapsulation layer reaching the interior caused device failure. Thus, the device output dropped to ≈0 V in liquid environment (Figure 3d). The initial output of the BTS in nonliquid environment (3.2 V) is higher than that in liquid environment (2 V) (Figure 3e). The attenuation of the output voltage is mainly due to the electrostatic shielding effect caused by liquid infiltration.

2.4. Antibacterial and Biocompatibility Properties

Antibacterial performance is essential for implantable medical devices to reduce the risk of infection. PLA/chitosan 4% was used as an encapsulation layer to impart certain antibacterial properties to the device. PLA/chitosan 4% has excellent antibacterial properties, and 99.9% of the bacteria are killed. As controls, the clean culture dish and the PLA group showed almost no antibacterial property, and a large number of colonies were produced on the culture plate (Figure 3f,g; and Figure S5, Supporting Information). In addition, the addition of chitosan did not change the output voltage of BTS significantly (Figure S6, Supporting Information).

Excellent biocompatibility and antibacterial properties are essential to avoid negative biological responses and infections.

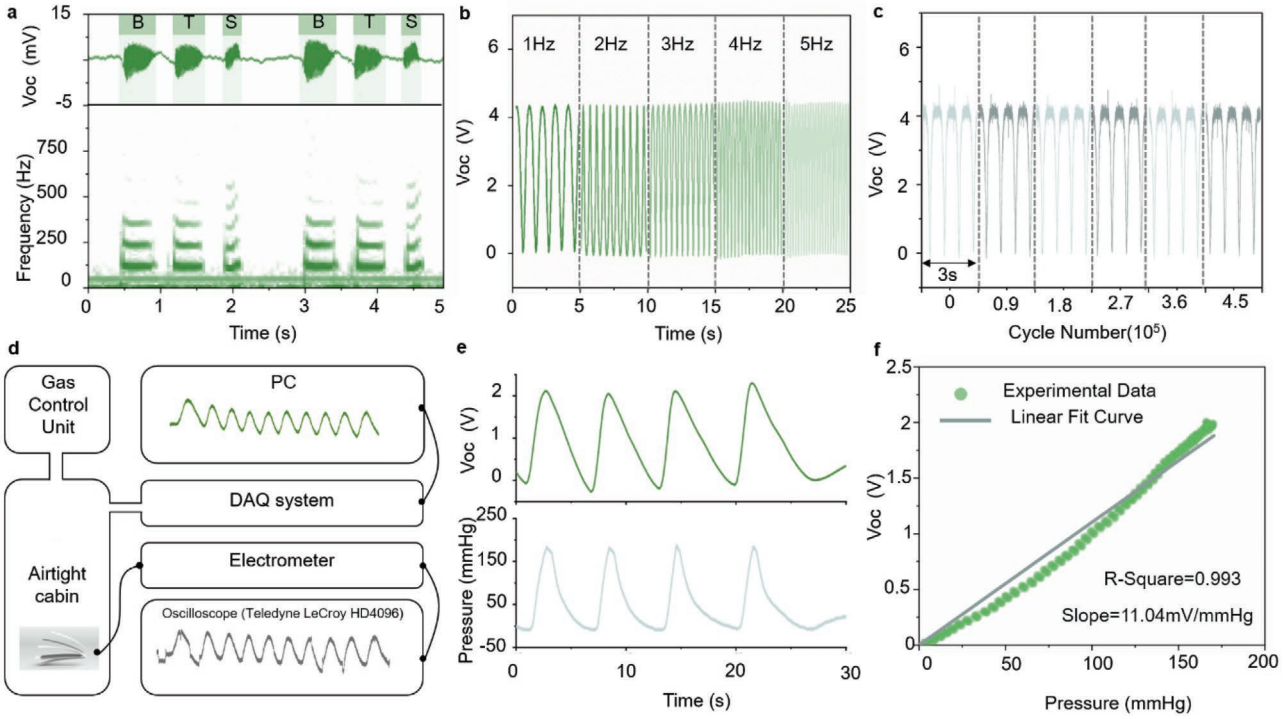

Figure 2. Performance of the BTS in vitro. a) Output voltage of the BTS (top) and spectrum analysis result (bottom) in vocal cord vibration monitoring. b) Open-circuit voltage of the BTS under different frequency load forces. c) Long-term stability tests of the BTS. d) Schematic diagram of the pressure simulation and testing system. e) Comparison between the pressures and the output voltages of the BTS. f) Overall linearity of the pressure and the output voltage of the BTS.

Here, the mass of all magnesium layer of BTS is ≈0.15 mg. The part of the Mg wire left in the body is about 1.3 mg. The rapid degradation of excessive magnesium may cause the surrounding environment to be alkaline, which may adversely affect surrounding cells and tissues. Thus, we studied the biocompatibility by observing the growth of mouse fibroblasts (L929) cocultured with BTS and BTS fragments. In the experimental and control groups, L929 had similar diffusion and adherent growth behavior, and the complete cell structure was detected (Figure S7, Supporting Information). The methyl thiazolyl tetrazolium (MTT) values of the experimental group and the control group were similar, and both increased well at 1, 2, and 3 days. These results confirm the good biocompatibility of the BTS (Figure 3h). No significant inflammatory reaction was observed in the histological section of tissue at 9 weeks (Figure S8 and Note S4, Supporting Information).

2.5. Abnormal Respiratory Event Identification in Small Animals

A biomechanical testing system was built to verify the sensing ability of the BTS (**Figure 4**a). The BTS was placed under the abdominal cavity skin, while a commercial mechanical sensor was placed in vitro as a reference (Figure 4b; and Figure S9a,b, Supporting Information). The process of contact-separation of triboelectric layers is along with the inhale and expiration of the thorax. The BTS is compressed in inhale, resulting in an increased output voltage. However, the pressure on the BTS is released in expiration, resulting in a reduced output voltage (Figure S10a,b, Supporting Information).

Abnormal respiratory events (dyspnea) are easily detected. When dyspnea occurs, which causes the overall thorax to decrease, but the amplitude of each breath increases. The BTS and commercial mechanical sensor are in and outside the body, respectively. Thus, the compression force on the BTS in the body is increased, while the compression force on the external commercial mechanical sensor outside the body is reduced (Figure 4c,d). In addition, the BTS can work stably in the body for 5 days. The encapsulation layer was damaged on the 6th day, and the liquid penetrated into the device, making it ineffective (Figure 4e).

2.6. Abnormal Cardiovascular Event Identification in Large Animals

The BTS was attached to the vascular wall, whereas the commercial sensors communicated with the inside of blood vessels through needle tips and catheters (**Figure 5**a,b; and Figure S11a–f, Supporting Information). The sensor signals have some differences due to the different placement positions. The ambulatory blood pressure signal obtained by the BTS has good consistency with commercial blood pressure sensors. Arrhythmia events can also be easily identified by the BTS (Figure 5c).

The process of contact-separation of triboelectric layers is along with the diastole and systole blood pressure phase. During the systolic blood pressure phase, the BTS is compressed by the blood vessel and leading to an increased output voltage. In the diastole blood pressure phase, the pressure on the BTS is released and leading to a reduced output voltage (Figure S12a,b, Supporting Information).

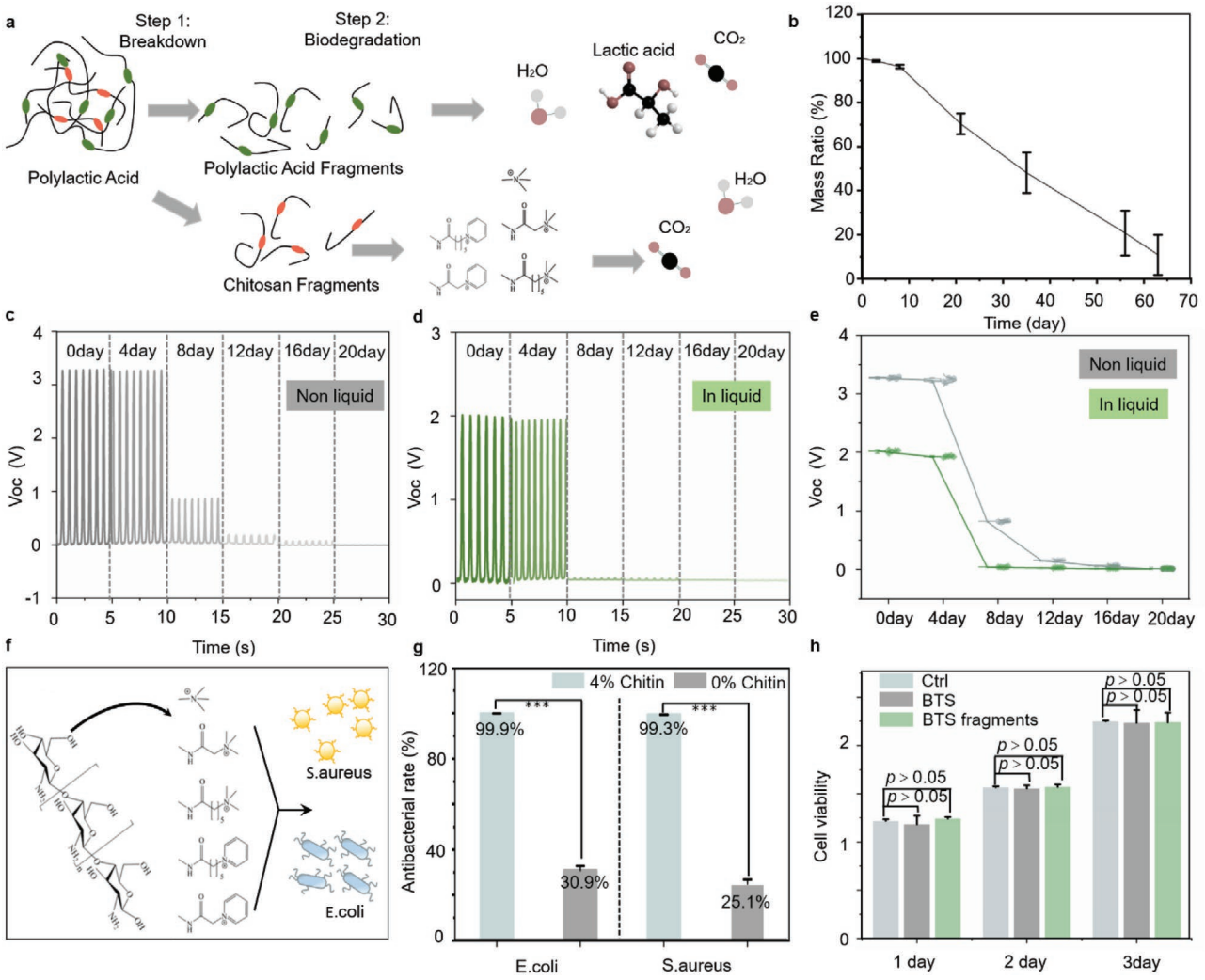

Figure 3. In vitro degradation performance and biocompatibility evaluation of the BTS, and sterilization results of PLA/C for *E. coli* and *S. aureus*. a) Illustration of biodegradation for PLA/C polymer (encapsulation layer material). b) Relationship between the mass ratio of the BTS and degradation time. c–e) Relationship between the open-circuit voltage of the BTS and degradation time in vitro and in vivo. f) Antibacterial effect on *E. coli* and *S. aureus* treated with PLA/C. g) Sterilization of the bacterial population for *E. coli* and *S. aureus*; the CFU was reduced significantly after PLA/C treatment. h) The viability of L929 cells after being cultured for 3 days. All data in (b,e,g,h) are presented as the mean ± SD.

To confirm the ability of the BTS to monitor abnormal vascular occlusion events, we constructed a vascular occlusion model through an implanted balloon. When the balloon is inflated, the blood vessel is blocked, and the blood pressure drops rapidly; then, the blood pressure is restored after deflating the balloon (Figure 5d). The BTS detected a total of 5 simulated blood vessel blockage events in the trial (Figure S13a–f, Supporting Information). There is great potential in the prognosis of cardiovascular surgery.

3. Conclusion

The long service life of the BTS demonstrated here is critical for postoperative care applications. Most implanted biodegradable sensors cannot meet the postoperative care cycle (≈4–10 days). A longer service life means a longer degradation/absorption time. Making devices compatible with long-term operation and rapid degradation is challenging.[22] Thus, a thinner stable encapsulation layer and a rapid degradation working layer are required. The service life of the BTS is 5 days, and the average complete degradation and absorption time is 84 days, which meets the requirements of cardiovascular surgery prognosis. Here, we suggest a service efficiency parameter to evaluate the performance of bioabsorbable or degradable devices. This service efficiency parameter is defined as the following equation

$$\text{Service efficiency} = \frac{\text{Service time}}{\text{Total degradation time}} \quad (2)$$

The service efficiency of the BTS is 5.95%.

The BTS offers good durability due to the structure design and material selection. The triboelectric device relies on contact separation to generate electrical signals. The pressure on

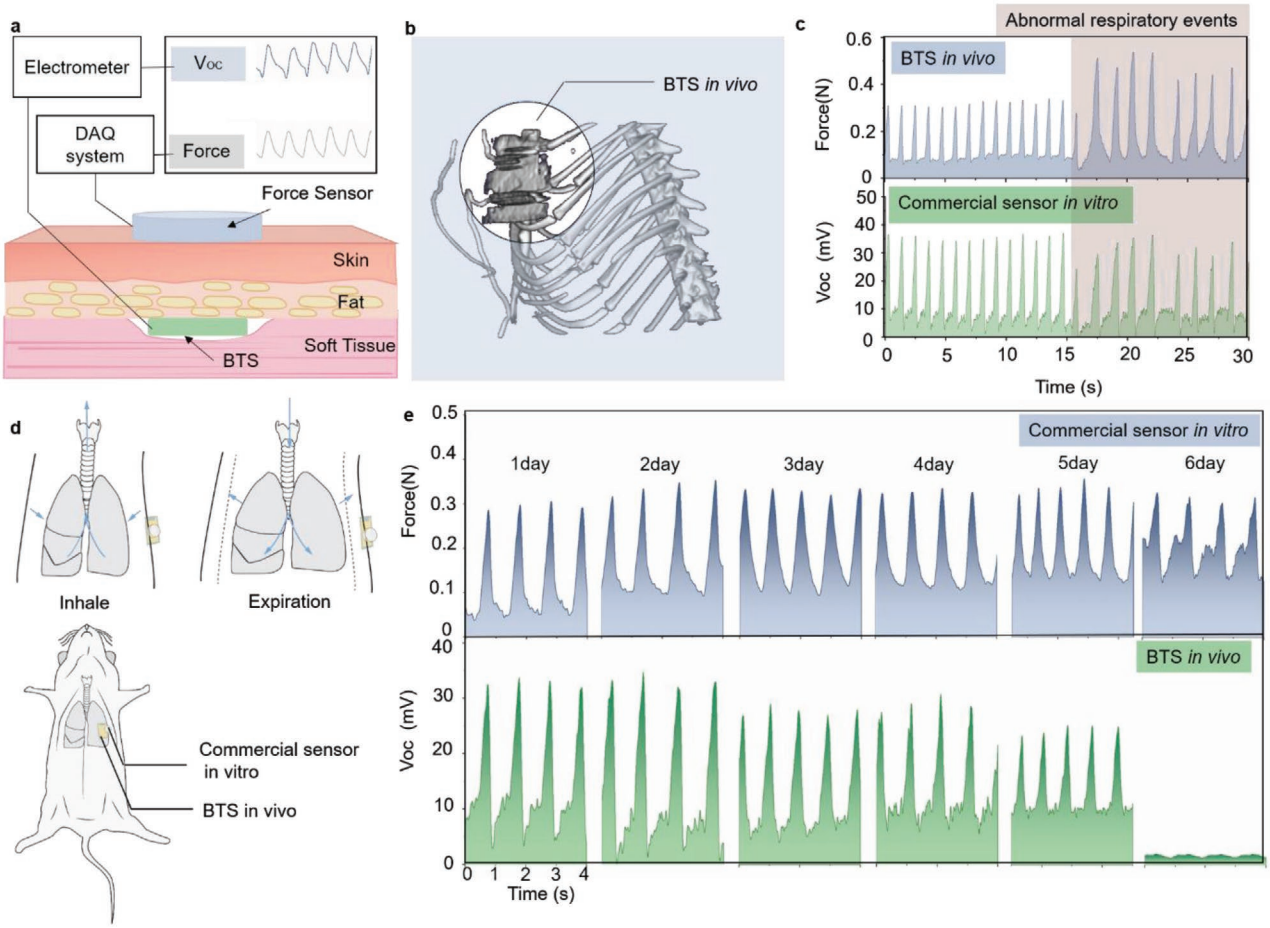

Figure 4. Abnormal respiratory event identification and in vivo performance test in a small animal. a) Diagram of the biomechanical testing system. b) Micro-CT image of a rat abdominal cavity implanted with a BTS. c) Abnormal respiratory events (dyspnea) are detected by the BTS and commercial sensors. d) Illustration of the in vivo performance test. e) Output of the BTS at several time intervals up to 6 days after implantation.

the device is relatively average and it is not easy to be damaged under large strain. However, output of piezoelectric device relies on degree of flexure with large local stress and easy lead to break (Table S2, Supporting Information). Therefore, BTS has advantages in sensitivity and durability compatibility.

Ultralow power consumption is a necessity for biodegradable devices.[23] Here, both low power consumption and high sensitivity have been achieved with the BTS. The BTS as an active device does not consume power. The self-powering ability of triboelectric sensors is key to attaining compatibility of ultrahigh sensitivity and low power consumption for biodegradable/bioresorbable sensors.

The improvement of linearity and measurement range is a challenge for triboelectric sensors. The previous triboelectric sensors with other spacer structures often have two linear ranges.[24] The first linear range has extremely high sensitivity but low measurable range. The second linear range has low sensitivity and wide measurable range. However, the overall linearity of these devices is limited. These devices are difficult to meet the requirement of biological pressure measurement. An air spacer structure is designed to improve the measurement range and linearity, which has higher linearity and measurement range than other spacer structures (Figure S14a–f, Supporting Information). Here, a smaller design distance between the triboelectric layers may lead to a lower output voltage (Table S3, Supporting Information).

The common antimicrobial strategies for implants surface have difficulty meeting the requirements of bioabsorbable devices. Here, the antibacterial property needs to apply to the entire BTS device from outside to inside. The antibacterial properties of the BTS can be maintained throughout degradation. This is a crucial aspect for the biosafety of bioresorbable devices that only employ medical materials commonly used in US Food and Drug Administration-approved implants for monitoring of biomechanical forces.

In summary, we have demonstrated a BTS. This is a self-powered sensor that is the first to achieve full bioresorbability in vivo and show the ability to identify abnormal disease events. The BTS can be absorbed and become part of the organism after the service life. The BTS offers advantages of excellent service efficiency (5.95%), antibacterial properties (99%), and output performance (2 V) and is expected to be applied in postoperative care as an in vivo bioresorbable electronic device (Table S4, Supporting Information).

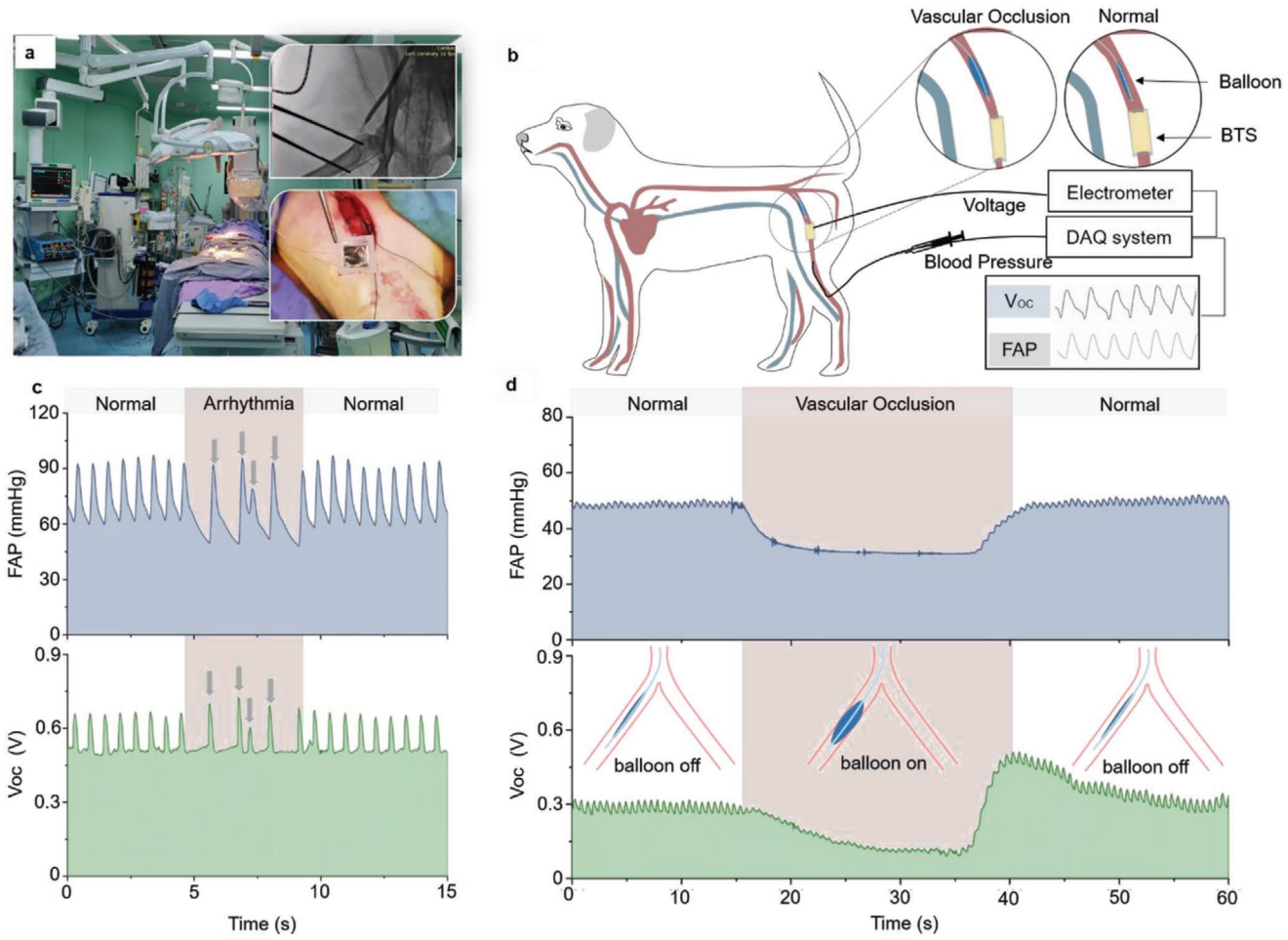

Figure 5. Abnormal cardiac event identification in a large animal. a) Image of the human-scale animal cardiac monitoring experiment. b) Schematic of in vivo experimental electrical characterization and physiological signal monitoring. c) Representative blood pressure indicating arrhythmia events corresponding to the output signal of the BTS. d) Simulated abnormal vascular occlusion events are detected by the BTS.

4. Experimental Section

Fabrication of the PLA/C Layer: PLA (Sigma-Aldrich) was dissolved in chloroform at a concentration of 5% w/v and stirred vigorously. Chiton (Sigma-Aldrich) solution was prepared in a 1% acetic acid solution and mixed with the PLA solution in a mass fraction of 4%. After no bubbles existed in the solution, it was cast on a glass plate for air drying. Then, it was placed in a heated oven for another 12 h to eliminate the remaining solvent. Plasma etching was applied to provide a micro–nanostructure on the PLA/C film.

Preparation of POC: POC was prepared using a previously described synthetic method.[25] Equimolar amounts of 1,8-octane diol and citric acid were mixed in a three-neck round-bottom flask fitted with an inlet and outlet adapter. The mixture was melted in a silicon oil bath at 165 °C. After the mixture temperature decreased to 140 °C, the mixture was stirred for another hour. The entire process was carried out under nitrogen gas with uniform stirring.

Fabrication of the BTS: The as-fabricated BTS contains triboelectric layers, electrodes, spacers, and encapsulation layers. In detail, a nanostructured PLA/C film was applied as the bottom triboelectric layer, and Mg (≈50 nm) deposited on the backside of PLA/C acted as one of the electrodes. A thin Mg film on a PLA/C film acted as both the top triboelectric film and another electrode. In addition, the spacers fabricated from POC were integrated into the PLA/C film to guarantee highly effective contact and separation. The structure mentioned above was encapsulated with a PLA/C film. It was further sealed by a heat sealer to exclude any interstices and ensure that the BTS was protected from the environment.

Electrical Measurement: All SEM images were obtained using a field-emission scanning electron microscope (Hitachi, SU8020) with preset parameters of 3 kV and 10 µA. The voltage, current, and charge transfer were measured by an electrometer (Keithley 6517B) and recorded by an oscilloscope (Teledyne LeCroy HD 4096) or data acquisition hardware (PowerLab 4/35). Mg wires (Mg 0.1 series JingJun Materials Technology Co. Ltd. (Suzhou China)) have been used as electrical connections. The high-temperature annealing method is used to make it form a MgO passivation layer. Then PLA/C coating is added to surface to improve its resistance to corrosion by phosphate buffer saline (PBS) solution. When the BTS is implanted in vivo, the part of the Mg wires left in the body (0.1 mm × 0.1 mm × 20 mm × 2) is about 1.3 mg.

Vocal Cord Vibration Monitoring: To demonstrate the dynamic mechanical sensing performance, the BTS was attached to the throat to monitor vocal cord vibration. The volunteer pronounced "B" "T" and "S." The voltage were measured by an electrometer (Keithley 6517B) and recorded by an oscilloscope (Teledyne LeCroy HD 4096). The study protocol was reviewed and approved by the Ethical Committee of Beijing Institute of Nanoenergy and Nanosystems (A-2019032). The informed consent of all participating subjects was obtained.

Calculation of Sensitivity: The sensitivity is employed to evaluate the BTS sensing performance. The sensitivity (S) can be derived from the following equation

$$S = \text{Slope}U_{OC}(P) = \frac{\Delta U_{oc}}{\Delta P} \quad (3)$$

Here, "Slope" is the slope function, U_{OC} is the open-circuit output voltage, and P is the load pressure.

In Vitro Pressure Test: The pressure testing system contains an airtight cabin, a gas control system, an electrometer, and commercial pressure measurement equipment (BIOPAC MP150, TSD104). The internal pressure of the confined chamber was monitored by a commercial probe and displayed using a data acquisition (DAQ) system. With the pressure in the confined chamber regulated by the gas control unit, the signals of the BTS were collected and compared with the data documented by the DAQ system as a reference standard.

In Vitro Force Test: The BTS was driven by a linear motor (frequency, 1–5 Hz; acceleration, 1 m s^{-2}; deceleration, 1 m s^{-2}; maximum speed, 1 m s^{-2}). The applied force was ≈20 N, as measured by a dynamometer (MARK-10-M7-2).

Accelerated Fatigue Test: A linear motor (RS01, LinMot) was employed as a source of mechanical stimuli (20 N, 1.35 Hz) for a saturated accelerated fatigue test. The output voltage of the BTS was measured within 10 s at intervals of 18.5 h which is approximately every 9×10^4 cycles. The measurement method is shown in the "In vitro force test" section.

High-Frequency Test: A small loudspeaker (HARMAN W54N8A) generates mechanical vibrations. A 1 kHz sinusoidal alternating current (10 V, 1 kHz) gave as the driving source. The maximum mechanical displacement caused by the 1 kHz loudspeaker is approach to 0.17 mm.

Degradation Performance of the BTS: To mimic the in vivo environment on BTS operation, the test environment was replaced with (1 × PBS), named in liquid environment. Here, the nonliquid environment is in a dry environment (relative humidity 40–50%). In addition, the accelerated degradation test of bioresorbable triboelectric sensor with Mg wires is performed in 1 × PBS at 90 °C (Figure S15, Supporting Information).

Cell Viability: The biocompatibility of the BTS was tested using a standard MTT (Sigma-Aldrich) assay through cell viability measurement. L929 cells were seeded at 1×10^6 per well in 6-well cell culture plates with and without the BTS. Until they adhered, they were incubated for another 1–3 days. Error bars are based on the standard deviations of at least quadruplicate measurements.

Cell Morphology and Immunofluorescent Staining: After being cultured for 1–3 days, the L929 cells in 6-well plates were fixed with immunohistochemistry fixation fluid (Beyotime) at room temperature for 30 min. After the samples were washed with 1 × PBS (pH 7.4) three times, they were further treated with 0.1% Triton X-100 for 10 min and blocked with 0.1% bovine serum albumin (BSA) solution for 1 h at 37 °C. Then, Alexa Fluor 594 phalloidin (1:40 dilution) and DAPI (1:400 dilution) were incubated for 1 h and 10 min, respectively. The immunofluorescence images were acquired using a Leica confocal fluorescence microscope (LECIA TCS SP8).

Antibacterial Property Test: The antibacterial activity of the samples was assessed with gram-positive (*Staphylococcus aureus*, 29213) and gram-negative (*Escherichia coli*, ATCC 25922) bacteria. The pure bacteria in LB were cultivated overnight in a rotating shaker at 37 °C and cultivated to a concentration of 10^9 CFU mL^{-1} (OD490 = 0.3 for *S. aureus* and OD600 = 1.0 for *E. coli*). The PLA and PLA-C films (1 × 1 cm) were immersed in the bacterial solution at a concentration of 10^7 mL^{-1} for 24 h. Meanwhile, blank groups with 10^7 mL^{-1} *S. aureus* or *E. coli* cultured for 24 h were applied as the control group. After removing the films, the bacterial solution was centrifuged at 8000 rpm, resuspended in PBS, and then uniformly inoculated on solid medium plates after gradient dilution. Colony counting was conducted after 24 h of culture in a constant temperature incubator at 37 °C.

Animal Experimentation: All the animal experiments in this work (the in vivo study and the abnormal respiratory and cardiovascular event identification experiments) were performed following ethical approval by the Ethical Committee of Animal Experimental Center in Fuwai Hospital (0100-3-2-ZX(Y)), and the procedure strictly followed the "Beijing Administration Rule of Laboratory Animals" and the national standards of "Laboratory Animal Requirements of Environment and Housing Facilities (GB14925–2001).

In Vivo Study: The BTS was implanted into the back of an SD rat. The biodegradation was measured using micro-CT for 0–12 weeks. Histological evaluation of the in vivo biocompatibility was performed. After 12 weeks of implantation, the BTS disappeared. The animal was euthanized, and myocardial tissues were excised from the implantation site. Tissue sections (5 µm) were prepared for histologic analysis including hematoxylin and eosin (H&E), Masson's trichrome and immunohistochemical staining.

Abnormal Respiratory Event Identification Experiment: To demonstrate that the BTS can work properly and efficiently in vivo, the BTS degradation after implantation into the abdominal cavity region of SD rats was evaluated.

Abnormal Cardiovascular Event Identification Experiment: The adult male beagle dog (15 kg) fasted for 12 h before surgery. Briefly, the animal was anesthetized with an injection of propofol (6 mg kg^{-1}, IV) and then intratracheally intubated and ventilated. Anesthesia was maintained with 2 mg kg^{-1} h^{-1} propofol during the surgery. A dynamic arterial pressure catheter was inserted into the right femoral artery and linked.

Statistical Analysis: Data were expressed as mean ± SD. The one-way ANOVA was used to compare mean values in groups of samples for all experiments. Error bars were calculated using mean ± SD. with a group size $n \geq 3$. All reported p values were calculated for groups with analysis of variance (one-Way ANOVA) using the Origin software programme. Reported p-values for all experiments correspond to $*p < 0.05$, $**p < 0.01$, $***p < 0.001$. The $*p < 0.05$ was considered significant.

Supporting Information

Supporting Information is available from the Wiley Online Library or from the author.

Acknowledgements

The authors are grateful to Dr. Xuecheng Qu, Dr. Xia Wang, Dr. Hu Li, and other laboratory members for their cooperation in this study. The authors thank the National Natural Science Foundation of China (Nos. 61875015, 62004010, U20A20390, and 11827803), National Postdoctoral Program for Innovative Talent (No. BX20190026), China Postdoctoral Science Foundation (No. 2019M660410), Beijing Natural Science Foundation (No. JQ20038), and The Fundamental Research Funds for the Central Universities for the support.

Conflict of Interest

The authors declare no conflict of interest.

Author Contributions

H.O., Z.L., and M.G. contributed equally to this work. Z.L., Z.L.W, H.O., Y.F., Z.L., and W.H. conceived the project. H.O., Z.L., and Z.Y. carried out the BTS fabrication and electrical characteristic work H.O., H.L., and Z.L. accomplished the material characterization. H.O., Z.L., M.G., Y.H., Y.D., and S.C. designed and carried out the large animal model experiment. H.O., Y.F., and Z.L. have processed the data and carried out the statistical analysis of the electrical signal. H.O., Z.L., W.H., G.M., Y.H., and D.J. analyzed the physiological signals from animal experiments. H.O., Z.L., B.S., M.G., and Y.H. wrote the manuscript, and all authors reviewed and commented on the manuscript.

Data Availability Statement

Research data are not shared.

Keywords

bioresorbable materials, dynamic pressure sensors, implantable devices, postoperative care, triboelectrics

Received: March 24, 2021
Revised: May 10, 2021
Published online: August 8, 2021

[1] a) F. R. Fan, W. Tang, Z. L. Wang, *Adv. Mater.* **2016**, *28*, 4283; b) Y. H. Jung, J. U. Kim, J. S. Lee, J. H. Shin, W. Jung, J. Ok, T. i. Kim, *Adv. Mater.* **2020**, *32*, 1907478.

[2] C. Li, C. Guo, V. Fitzpatrick, A. Ibrahim, M. J. Zwierstra, P. Hanna, A. Lechtig, A. Nazarian, S. J. Lin, D. L. Kaplan, *Nat. Rev. Mater.* **2020**, *5*, 61.

[3] S.-K. Kang, R. K. Murphy, S.-W. Hwang, S. M. Lee, D. V. Harburg, N. A. Krueger, J. Shin, P. Gamble, H. Cheng, S. Yu, *Nature* **2016**, *530*, 71.

[4] Q. Zheng, Y. Zou, Y. Zhang, Z. Liu, B. Shi, X. Wang, Y. Jin, H. Ouyang, Z. Li, Z. L. Wang, *Sci. Adv.* **2016**, *2*, e1501478.

[5] N. Rajgor, M. Patel, V. Bhaskar, *Surg. Neurol. Int.* **2011**, *2*, 91.

[6] E. J. Curry, K. Ke, M. T. Chorsi, K. S. Wrobel, A. N. Miller, A. Patel, I. Kim, J. Feng, L. Yue, Q. Wu, *Proc. Natl. Acad. Sci. USA* **2018**, *115*, 909.

[7] E. J. Curry, T. T. Le, R. Das, K. Ke, E. M. Santorella, D. Paul, M. T. Chorsi, K. T. Tran, J. Baroody, E. R. Borges, *Proc. Natl. Acad. Sci. USA* **2020**, *117*, 214.

[8] a) X. Chen, J. A. Rogers, S. P. Lacour, W. Hu, D.-H. Kim, *Chem. Soc. Rev.* **2019**, *48*, 1431; b) R. Feiner, T. Dvir, *Nat. Rev. Mater.* **2017**, *3*, 17076.

[9] a) Y. J. Hong, H. Jeong, K. W. Cho, N. Lu, D. H. Kim, *Adv. Funct. Mater.* **2019**, *29*, 1808247; b) Y. Song, J. Min, W. Gao, *ACS Nano* **2019**, *13*, 12280.

[10] Y. H. Jung, T.-H. Chang, H. Zhang, C. Yao, Q. Zheng, V. W. Yang, H. Mi, M. Kim, S. J. Cho, D.-W. Park, *Nat. Commun.* **2015**, *6*, 7170.

[11] a) M. Irimia-Vladu, *Chem. Soc. Rev.* **2014**, *43*, 588; b) M. Baumgartner, F. Hartmann, M. Drack, D. Preninger, D. Wirthl, R. Gerstmayr, L. Lehner, G. Mao, R. Pruckner, S. Demchyshyn, *Nat. Mater.* **2020**, *19*, 1102; c) W. B. Han, J. H. Lee, J. W. Shin, S. W. Hwang, *Adv. Mater.* **2020**, *32*, 2002211; d) W. Li, Q. Liu, Y. Zhang, C. Li, Z. He, W. C. Choy, P. J. Low, P. Sonar, A. K. K. Kyaw, *Adv. Mater.* **2020**, *32*, 2001591.

[12] a) M. T. Chorsi, E. J. Curry, H. T. Chorsi, R. Das, J. Baroody, P. K. Purohit, H. Ilies, T. D. Nguyen, *Adv. Mater.* **2019**, *31*, 1802084; b) S. W. Hwang, G. Park, H. Cheng, J. K. Song, S. K. Kang, L. Yin, J. H. Kim, F. G. Omenetto, Y. Huang, K. M. Lee, *Adv. Mater.* **2014**, *26*, 1992; c) D.-H. Kim, J. Viventi, J. J. Amsden, J. Xiao, L. Vigeland, Y.-S. Kim, J. A. Blanco, B. Panilaitis, E. S. Frechette, D. Contreras, *Nat. Mater.* **2010**, *9*, 511.

[13] M. Choudhury, *Clin. Surg.* **2017**, *2*, 1584.

[14] B. Zhu, H. Wang, W. R. Leow, Y. Cai, X. J. Loh, M. Y. Han, X. Chen, *Adv. Mater.* **2016**, *28*, 4250.

[15] H. Li, C. Zhao, X. Wang, J. Meng, Y. Zou, S. Noreen, L. Zhao, Z. Liu, H. Ouyang, P. Tan, *Adv. Sci.* **2019**, *6*, 1801625.

[16] a) F.-R. Fan, Z.-Q. Tian, Z. L. Wang, *Nano Energy* **2012**, *1*, 328; b) Z. L. Wang, J. Song, *Science* **2006**, *312*, 242.

[17] a) Z. Li, G. Zhu, R. Yang, A. C. Wang, Z. L. Wang, *Adv. Mater.* **2010**, *22*, 2534; b) Q. Zheng, B. Shi, F. Fan, X. Wang, L. Yan, W. Yuan, S. Wang, H. Liu, Z. Li, Z. L. Wang, *Adv. Mater.* **2014**, *26*, 5851; c) H. Ouyang, J. Tian, G. Sun, Y. Zou, Z. Liu, H. Li, L. Zhao, B. Shi, Y. Fan, Y. Fan, *Adv. Mater.* **2017**, *29*, 1703456.

[18] a) Q. Zheng, Q. Tang, Z. L. Wang, Z. Li, *Nat. Rev. Cardiol.* **2020**, *18*, 7; b) H. Wang, L. Xu, Y. Bai, Z. L. Wang, *Nat. Commun.* **2020**, *11*, 4203.

[19] a) R. Wang, S. Gao, Z. Yang, Y. Li, W. Chen, B. Wu, W. Wu, *Adv. Mater.* **2018**, *30*, 1706267; b) H. J. Kim, J. H. Kim, K. W. Jun, J. H. Kim, W. C. Seung, O. H. Kwon, J. Y. Park, S. W. Kim, I. K. Oh, *Adv. Energy Mater.* **2016**, *6*, 1502329; c) X. Peng, K. Dong, C. Ye, Y. Jiang, S. Zhai, R. Cheng, D. Liu, X. Gao, J. Wang, Z. L. Wang, *Sci. Adv.* **2020**, *6*, eaba9624.

[20] a) H. Zou, L. Guo, H. Xue, Y. Zhang, X. Shen, X. Liu, P. Wang, X. He, G. Dai, P. Jiang, H. Zheng, B. Zhang, C. Xu, Z. L. Wang, *Nat. Commun.* **2020**, *11*, 2093; b) S. Lin, L. Xu, A. C. Wang, Z. L. Wang, *Nat. Commun.* **2020**, *11*, 399; c) H. Zou, Y. Zhang, L. Guo, P. Wang, X. He, G. Dai, H. Zheng, C. Chen, A. C. Wang, C. Xu, Z. L. Wang, *Nat. Commun.* **2019**, *10*, 1427; d) S. Chao, H. Ouyang, D. Jiang, Y. Fan, Z. Li, *EcoMat.* **2021**, *3*, e12072.

[21] J. Peng, S. D. Kang, G. J. Snyder, *Sci. Adv.* **2017**, *3*, eaap8576.

[22] M. A. Woodruff, D. W. Hutmacher, *Prog. Polym. Sci.* **2010**, *35*, 1217.

[23] a) M. Tsang, A. Armutlulu, A. W. Martinez, S. A. B. Allen, M. G. Allen, *Microsyst. Nanoeng.* **2015**, *1*, 15024; b) X. Huang, D. Wang, Z. Yuan, W. Xie, Y. Wu, R. Li, Y. Zhao, D. Luo, L. Cen, B. Chen, *Small* **2018**, *14*, 1800994.

[24] a) L.u Zhaoxian, Z. Zhizhen, Z. Xiangwen, F. Xiuli, H. Youfan, *Nano Energy* **2019**, *59*, 295; b) L. Lin, Y. Xie, S. Wang, W. Wu, S. Niu, X. Wen, Z. L. Wang, *ACS Nano* **2013**, *7*, 8266.

[25] a) J. Yang, A. R. Webb, G. A. Ameer, *Adv. Mater.* **2004**, *16*, 511; b) C. G. Jeong, S. J. Hollister, *J. Biomed. Mater. Res., Part B* **2010**, *93*, 141.